TIME-AVERAGED HOLOGRAPHIC INTERFEROMETRY, APPLIED TO THE VIBRATION ANALYSIS OF HIGH FREQUENCY LOUD-SPEAKER CONES

by

WOLFGANG JOACHIM HARTMANN, B.Sc.

PART B: McMASTER(ON-CAMPUS) PROJECT*

A Report
Submitted to the School of Graduate Studies
in Partial Fulfilment of the Requirements
for the Degree
Master of Engineering

April 1976

*One of two Project Reports: The other part is designated PART A: McMASTER(Off-CAMPUS) Project

MASTER OF ENGINEERING (1976) McMASTER UNIVERSITY
Department of Engineering Physics Hamilton, Ontario

TITLE: TIME-AVERAGED HOLOGRAPHIC INTERFEROMETRY, APPLIED TO THE VIBRATION ANALYSIS OF HIGH FREQUENCY LOUD-SPEAKER CONES

AUTHOR: WOLFGANG JOACHIM HARTMANN, B.Sc. (Calgary, Alberta)

SUPERVISOR: Dr. E.A. Ballik

NUMBER OF PAGES: ix, 51

ABSTRACT

Time-averaged holographic interferometry is applied to the study of the resonance mode structures of an electromagnetic and a piezoelectric high frequency loud-speaker. Vibrational amplitude measurements were made using the simple concept of the holo-diagram. The vibrational amplitude sensitivity range was from 0.1 μm to 0.9 μm, which was an ideal range since the speaker vibrational amplitudes were always below 0.8 μm. Application of the technique to non-destructive speaker quality testing and optimum speaker design is also discussed in the report.

ACKNOWLEDGEMENTS

The author wishes to thank Dr. E.A. Ballik, Department of Engineering Physics, for his guidance in the preparation of this project. The technical assistance of Mr. G. Leinweber and Mr. A. Singh is also greatly appreciated.

TABLE OF CONTENTS

LIST OF FIGURES

LIST OF TABLES

CHAPTER 1

INTRODUCTION

Since the invention of the laser, holography has become an important tool in optical data processing, displays, microscopy, information storage, and interferometry.[1-6] In holographic interferometry the holographic image interferes with an object or another holographic image. The interference fringes are therefore produced by differing optical paths of two object beams. The amount by which the two paths differ then determines whether the beams interfere constructively, producing a light fringe, or destructively, producing a dark fringe.

The difference in optical path can be achieved in several ways. One way is to change the position of the illuminating object beam. Another is to immerse the object in a medium of different refractive index, which effectively changes the wavelength of one object beam. Both methods can be used to obtain contour maps of an object. Each dark interference fringe will therefore define a contour-line of constant depth.[1] The optical path is also changed when the object, or part of it, is displaced. This technique is of considerable importance in non-destructive material testing.[3,4,5]

Holographic interferometry basically consists of three interrelated methods:

(i) real-time holographic interferometry,

(ii) time-lapse holographic interferometry,

(iii) time-averaged holographic interferometry.

Real-time interferometry consists of first taking a regular hologram of an object and then returning the developed hologram and the object to the original positions (within a fraction of the wavelength of the illuminating light used). Now the hologram and the object are illuminated by the original reference and object beams, respectively. This creates two superimposed object beams; one from the holographic reconstruction, the other from the real illumination of the object. Depending on the magnitude of the displacement of the real object, the two object beams will interfere constructively or destructively. Any displacement or deformation of the object can, therefore, be detected as it happens, to an accuracy of a fraction of the wavelength of the laser light used for illumination. In time-lapse interferometry (or double-exposure holography) a hologram is made before and after an object's displacement or deformation on the same photographic plate, but before development of the plate. Again two interfering object beams are created. Time-lapse interferometry can be considered as taking a snapshot of real-time interferometry.

Time averaged interferometry, thoroughly treated by R.L. Powell and K.A. Stetson,[6] is primarily used to study rapid vibrations of small amplitudes. This technique can be compared to the time exposure of a swinging pendulum in ordinary photography. The pendulum spends most of its time at the two extremes of its swing, producing recognizable images at these locations. Holograms made with exposure times much longer than the object's period of vibration will, most of the

time, record wavefronts originating at the two extremes of the object's vibratory motion. A time-averaged hologram therefore closely approxmates a double exposed hologram recorded at the object's positions of maximum vibrational amplitude. The interference fringes produced will be a precise measure of the absolute value of the vibrational amplitude. Modes are readily visible as bright areas. Since no displacement is possible, these areas are just regular holograms. In the following study the emphasis will be on time-averaged holographic interferometry, applied to the cone vibrations of several small high frequency loudspeakers.

CHAPTER 2

HOLOGRAPHIC INTERFEROMETRY THEORY

2.1 Basic Holographic Principles

Holography is the reconstruction of three dimensional images and a hologram is the record of such an image. The discoverer, Dennis Gabor, demonstrated that a wavefront could be recorded not only in amplitude, as in conventional photography, but also in phase by interfering it with a background wave. A hologram is therefore a record of the interference of a reference beam coming directly from a coherent light source, and an object beam, which is a coherent light beam from the same source, but scattered by an object. The basic recording set-up is illustrated by Fig. 1. Let A be the total field recorded by a photosensitive medium, and let A_r and A_o be the fields of the reference beam and the object beam respectively. A is related to A_r and A_o by Eq. (2.1):[7]

$$A = A_r + A_o, \tag{2.1}$$

where A can be a complex amplitude. The total intensity of the radiation field can therefore be expressed by

$$I = AA^* = (A_r + A_o)(A_r + A_o)^*, \tag{2.2}$$

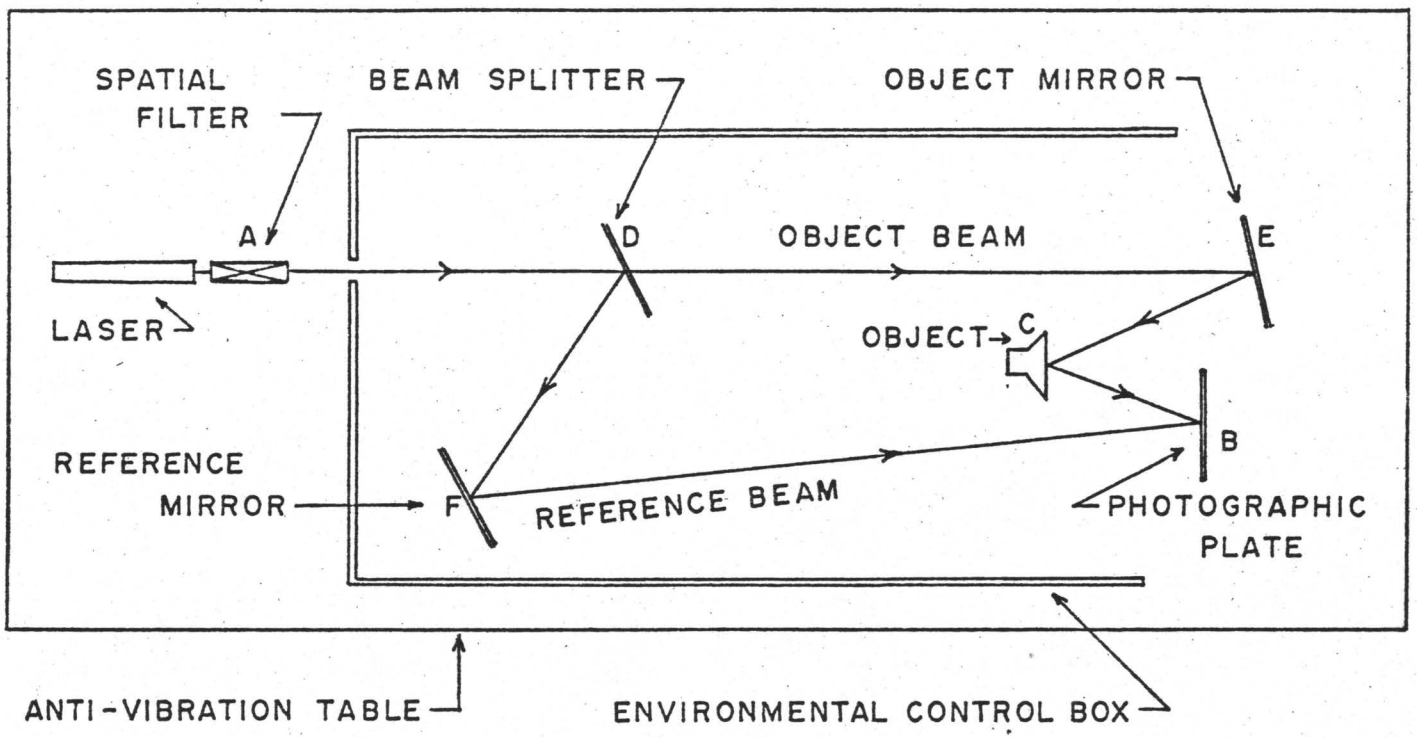

Fig. 1: Schematic Representation of the laboratory holographic setup

or

$$I = (A_r A_r^* + A_o A_o^* + A_o A_r^* + A_r A_o^*). \tag{2.3}$$

The intensities of the reference and object beam are given by I_r and I_o, respectively where I_r is given by

$$I_r = A_r A_r^*, \tag{2.4}$$

and I_o by

$$I_o = A_o A_o^*. \tag{2.5}$$

Using Eq. (2.4) and Eq. (2.5) we can rewrite Eq. (2.3) as

$$I = (I_r + I_o + A_o A_r^* + A_r A_o^*). \tag{2.6}$$

This intensity, I, is proportional to the change in the amplitude transmittance of the holographic recording, T, thus we obtain

$$T = k(I_r + I_o + A_o A_r^* + A_r A_o^*). \tag{2.7}$$

For reconstruction of the holographic image, the holographic recording is now illuminated by the reference beam, A_r, which is modified by the holographic recording transmittance, T, to give the transmitted radiation field:

$$R = A_r T = k[(I_r + I_o)A_r + A_o A_r A_r^* + A_r A_r A_o^*], \tag{2.8}$$

or

$$R = k[(I_r + I_o)A_r + A_o I_r + A_r A_r A_o^*]. \tag{2.9}$$

The first term of Eq.(2.9) is proportional to the field of the reference beam, the second term is proportional to the field of the object beam, while the third term can be regarded as undesirable noise. The second term is therefore a reconstruction of the original object beam and forms the holographic image.

2.2 General Holographic Interferometry Theory

Several theories have been developed for the practical interpretation of holographic interference patterns due to object surface displacements.[6,7,11-14] The following analysis is limited to time-averaged holographic interferometry.

The term which produces the reconstructed object beam in Eq. (2.9) can be defined by[7]

$$A_{or} = kI_r A_o, \tag{2.10}$$

or

$$A_{or} = C_1 A_o, \tag{2.11}$$

where C_1 is a constant proportional to the intensity of the reference beam. Since the object is vibrating, A_o has to be time-averaged. Therefore Eq. (2.11) can be written as

$$A_{or} = c_1 \frac{1}{t} \int_0^t A_o(t)dt, \tag{2.12}$$

where t is the exposure time. Using the Fresnel-Kirchhoff theory, Eq. (2.12) can be rewritten in the form:

$$A_{or} = \frac{C_1}{t} \int_0^t \iint_S S(x_o + x', y_o + y', z') \exp\left[\frac{2\pi i}{\lambda} r(t)\right] d(x_o + X') d(y_o + y') dt. \tag{2.13}$$

Here the double integral defines the object field A_o in the recording plane in terms of the object function S, where x_o, y_o, and z_o, are the average coordinates of a point on the object (z_o is taken as zero) and x', y', and z' are the time dependent variations about that position. The wavelength of the illuminating radiation is λ and r(t) is defined as the path of object beam distance between the object and the recorder, given by

$$r(t) = [(x - x_o - x')^2 + (y - y_o - y')^2 + (z - z')^2]^{\frac{1}{2}}, \tag{2.14}$$

where x, y, and z define the position of a point on the recorder. We now assume that the object beam is parallel to the z-direction and that the displacements of the object are small compared to the object-recorder distance. The object-recorder distance therefore can be approximated by z. Therefore we can conclude that $z >> z'$, $(x - x_o - x')^2 << z^2$, and $(y - y_o - y')^2 << z^2$. Using the binomial expansion, the path of the object beam between object and recorder can be written as

$$r(t) \approx z - z' + \frac{(x - x_o - x')^2}{2z} + \frac{(y - y_o - y')^2}{2z} . \qquad (2.15)$$

We now assume that all vibrations occur in the z-direction, parallel to the object beam, therefore, $x' = y' = 0$. The simplified forn of Eq. (2.13) therefore becomes

$$A_{or} = \frac{C_2}{t} \int_o^t \iint_s S(x_o,y_o,z')\exp[\frac{2\pi i}{\lambda} z']\exp[\frac{\pi i(x - x_o)^2}{\lambda z}]$$

$$\exp[\frac{\pi i(y - y_o)^2}{\lambda z}]dx_o dy_o dt. \qquad (2.16)$$

Here the constant, C_2 includes the term related to the object-recorder distance. Since z' is small, the surface function $S(x_o,y_o,z')$ can be approximated by $S(x_o,y_o,0)$, which is constant with respect to time. Equation (2.16) can therefore be written as

$$A_{or} = C_3 \int_o^t \exp[\frac{2\pi i}{\lambda} z']dt, \qquad (2.17)$$

where

$$C_3 = \frac{C_2}{t} \iint_s S(x_o,y_o,0)\exp[\frac{\pi i(x - x_o)^2}{\lambda z}]\exp[\frac{\pi i(y - y_o)^2}{\lambda z}]dx_o dy_o. \qquad (2.18)$$

For a sinusoidally vibrating object, z' can be written as

$$z'(t) = 2m\cos\omega t, \qquad (2.19)$$

where m is the vibrational amplitude and ω the frequency. Combining Eq. (2.17) and Eq. (2.19) we obtain

$$A_{or} = C_3 \int_o^t \exp[\frac{4\pi i}{\lambda} m\cos\omega t]dt. \tag{2.20}$$

The solution of the integral in Eq. (2.20) is the zero-order Bessel function. Therefore

$$A_{or} = C_3 J_o(\frac{4\pi m}{\lambda}). \tag{2.21}$$

The intensity of the reconstructed object beam may therefore be written as

$$I_{or} = C_4 J_o^2(\frac{4\pi m}{\lambda}), \tag{2.22}$$

where $C_4 = C_3^2$.

By a simple geometrical argument of the change in optical path length, as illustrated in Fig. 2, Eq. (2.22) can be altered to include object beams which are not parallel to the direction of vibration. This results in

$$I_{or} = C_4 J_o^2(\frac{4\pi m\cos\theta}{\lambda}), \tag{2.23}$$

where m is the vibrational amplitude in the direction of the angular bisector of the angle, 2θ, defined by the incident object beam and the scattered object beam, as shown in Fig. 2. Clearly, Eq. (2.22) is

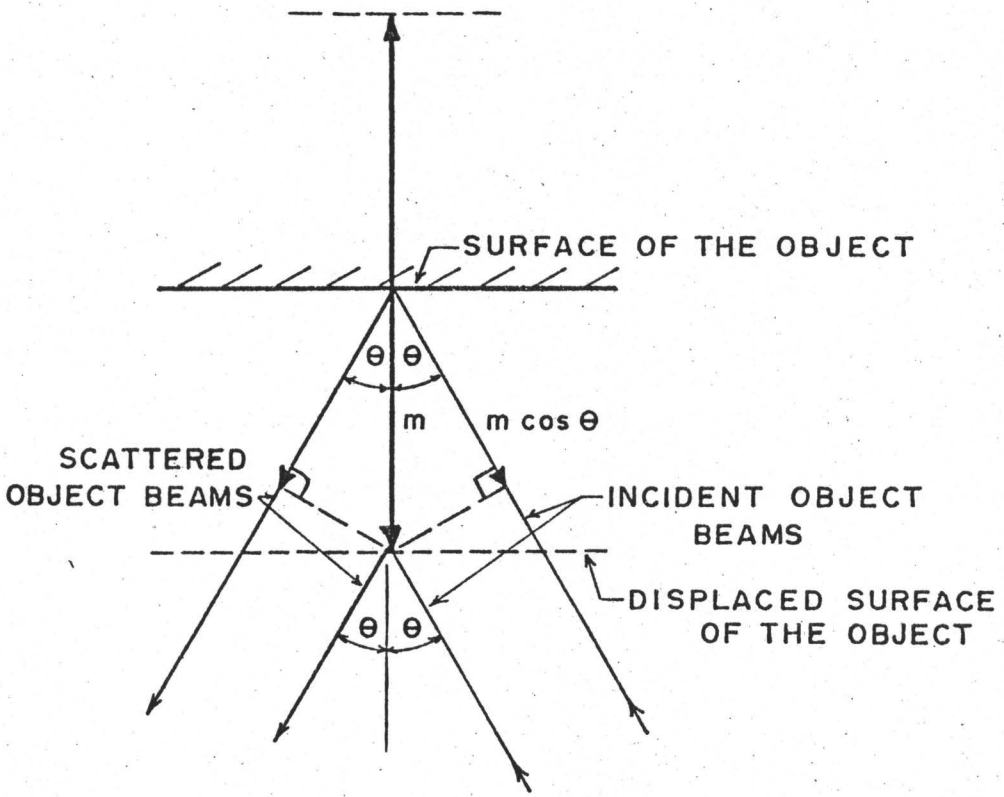

Fig. 2: The objects displacement with respect to the object beam

recovered when θ is zero. Dark interference fringes will therefore be produced whenever the Bessel intensity weighting function is zero. To make Eq. (2.23) conceptually more accessible, a holo-diagram[8,9] can be constructed, as shown in Fig. 3.

2.3 Analysis of the General Holographic Interferometry Theory

The use of the holo-diagram[8,9,10] considerably simplifies the maximization and interpretation of holographic interference patterns. This diagram consists of a set of ellipses with A and B as common focuses (see Fig. 3). For each ellipse, the path length between A and B, via a point C located anywhere on the same ellipse, is constant. Let A be the origin of the divergent laser beam, such as a spatial filter, and let B be the point of observation, which is usually a photographic plate. Then point C can be considered as the scattering object, Fig. 1. The circular arcs or "k-lines" in Fig. 3 are positions of constant sensitivity to vibrations perpendicular to the ellipses. The parameter k is defined by

$$k = (\cos\theta)^{-1}. \tag{2.24}$$

As before 2θ is defined as the angle between the incident object beam, $\overline{AC}$, and the scattered beam, $\overline{CB}$, subject to the condition that θ is the angle between the incident object beam and the normal of the ellipse at C.

The difference in optical pathlengths between two ellipses is given by

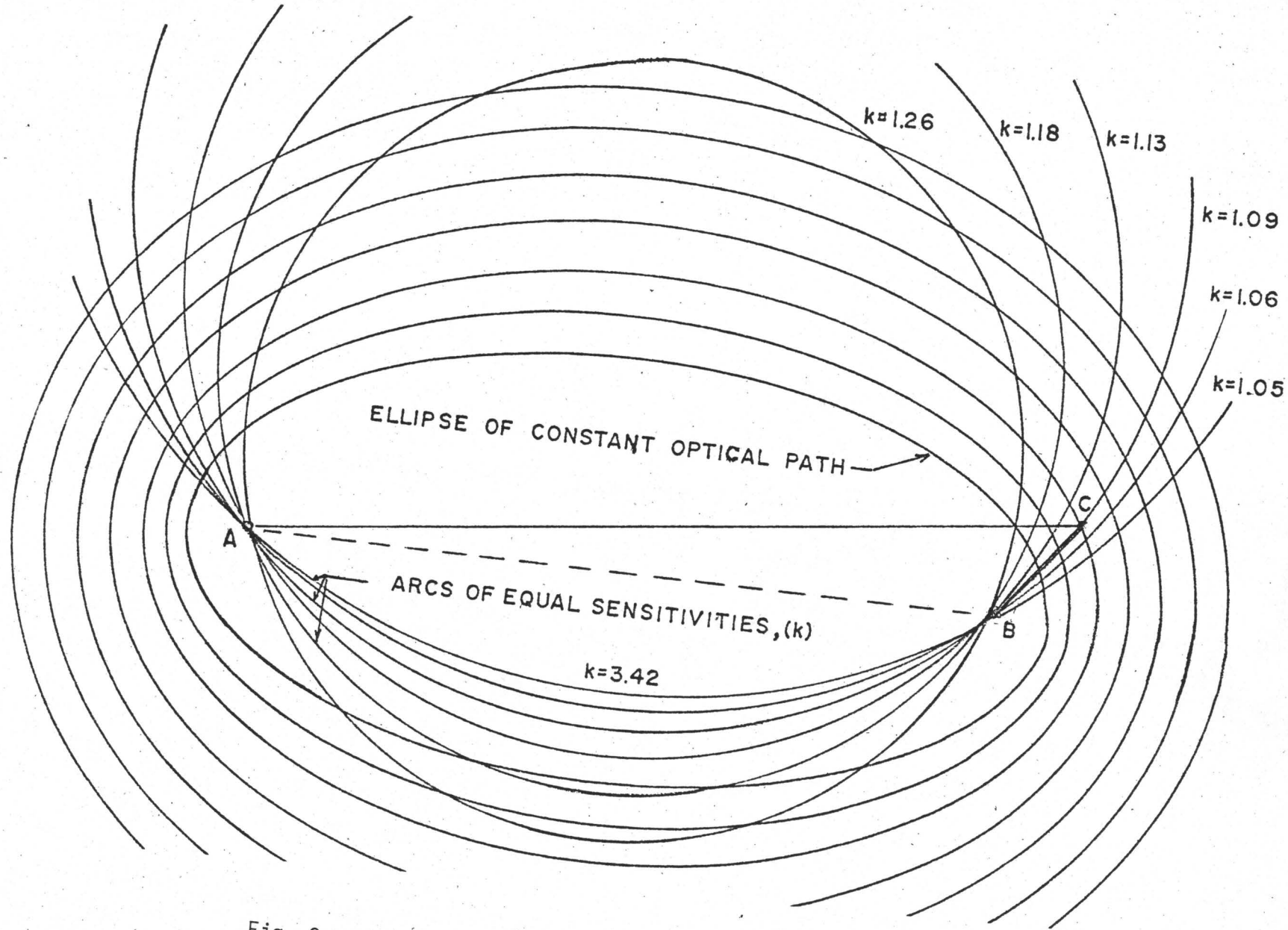

Fig. 3: The Holo-diagram

$$\Delta O = (\overline{A_o C_o} + \overline{C_o B_o}) - (\overline{A_1 C_1} + \overline{C_1 B_1}), \tag{2.25}$$

where subscripts refer to the two ellipses. Consider that the difference ΔO is sufficient to produce destructive interference. Then for small displacements, the point C_o (Fig. 4) on the original ellipse can be displaced to any point C_{1n} on the final ellipse. This means that we are only able to measure the displacement component perpendicular to the original ellipse at C_o. The real displacement can therefore be calculated only when its direction is known. The real amplitude of vibration is thus given by

$$m_r = m(\cos\alpha)^{-1}, \tag{2.26}$$

where α is the angle between the direction of vibration and the normal of the ellipse at C_o. From Fig. 3, we can see that the maximum sensitivity is obtained when C falls on the line $\overline{AB}$, since there the distance between adjacent ellipses is minimum. This corresponds to k = 1.

Destructive interference occurs whenever the reconstructed intensity, I_{or} (Eq. (2.23)) becomes zero. Therefore

$$J_o(X_n) = 0, \tag{2.27}$$

where X_n are the roots of the zero-order Bessel function. Combining Eq. (2.27) with Eq. (2.23) results in

$$X_n = \frac{4\pi m\cos\theta}{\lambda}, \tag{2.28}$$

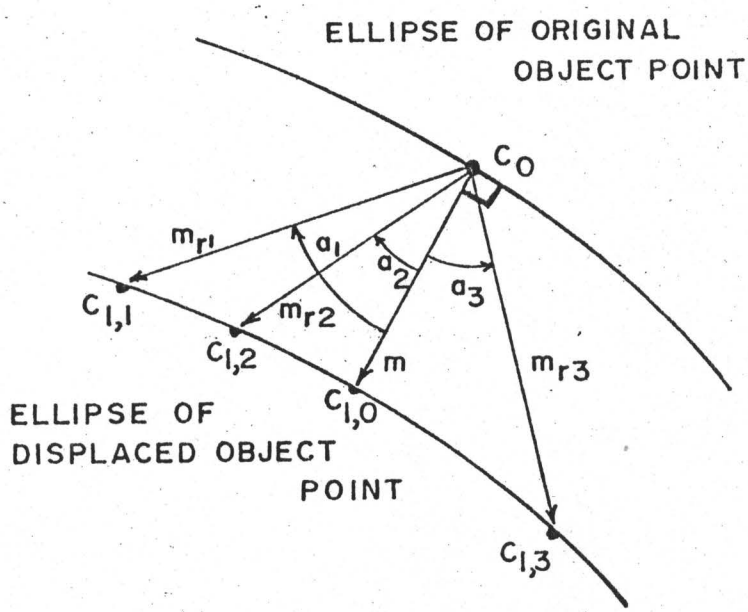

Fig. 4: The relative sensitivity of interferometric measurements from the holo-diagram point of view

or

$$m = \frac{X_n \lambda k}{4\pi} . \tag{2.29}$$

Using Eq. (2.29), Eq. (2.26) can be rewritten as

$$m_r = \frac{X_n \lambda k}{4\pi \cos\alpha} . \tag{2.30}$$

A He-Ne laser is a common coherent light source and the one used in this study. It is therefore convenient to introduce the factor

$$X_{nHe} = \frac{X_n \lambda_{He}}{4\pi} . \tag{2.31}$$

The real amplitude of vibration is therefore given by

$$m_{rHe} = X_{nHe} k (\cos\alpha)^{-1}, \tag{2.32}$$

where n is defined as the order of the destructive interference fringe, counted from locations on the object where nodes (i.e., zero displacements) occur. The factor, X_{nHe}, is tabulated in Table I. With the help of Eq. (2.32) and an appropriate holo-diagram, Fig. 3, the majority of holographic problems can be easily solved.

Table I

Dependence of the interferometric parameter, X_{nHe} on the interference fringe number

X_{nHe} (λ_{He} = 0.6328 μm),(μm)	Destructive interference fringe number
0.1211	1
0.2780	2
0.4358	3
0.5938	4
0.7519	5
0.9100	6
1.0681	7
1.2263	8
1.3844	9
1.5426	10

CHAPTER 3

THE ANALYSIS OF HIGH FREQUENCY LOUDSPEAKER CONE VIBRATIONS

3.1 Introduction

Before the discovery of holographic interferometry, investigations of loudspeaker cone vibrations was mainly done with a capacitor probe.[16] However some studies were done using stroboscopes and microphones.[15] When using the capacitance method, the cone is first sprayed with a thin coating of conductor. This coating and a small metallic probe form the two elements of a capacitor, as shown in Fig. 5. As the cone vibrates, the plate spacing of the capacitor is varied, which produces a signal voltage across R. The waveform of this voltage is then displayed on the cathode ray oscilloscope (CRO). The major disadvantage of this method is clearly the small area of vibrating cone that can be investigated at a given time. Holographic interferometry completely remedies this limitation. In addition, the vibrational amplitudes of the whole speaker can be recorded at the same time, with an accuracy of a fraction of a wavelength of the illuminating light source. Holographic interferometry can therefore be used to study even the small amplitude vibrational modes of high frequency loudspeakers.

3.2 Mode Structure of a Vibrating Cone

Exact mathematical solutions for vibrational modes can only be obtained for cylindrical and spherical shells and disks. Any information

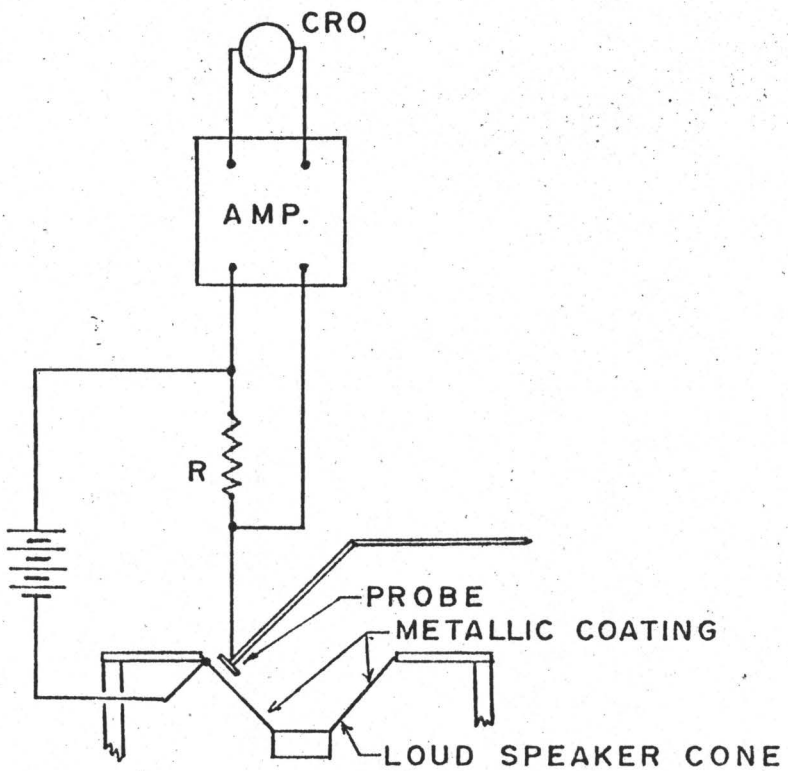

Fig. 5: Schematic representation of the capacitor method for cone vibration studies

concerning the vibrational modes of conical cones, therefore, has to be obtained by experimental measurements or by using solvable geometries as an approximation for the cone.[15]

There are two major types of vibrational modes pertaining to conical shells.

(i) radial modes as shown in Fig. 6a. These are associated with bending as, for example, in a ringing bell.

(ii) symmetrical or circular modes as shown in Fig. 6b. These are bending and extension as, for example, in a disk.

Both types of vibration can exist just by themselves or they can be superimposed to form a pattern with combined radial and circular mode characteristics.

3.3 Resonance Frequencies of Mode Structures

Whenever a speaker is driven at a mode producing frequency, called a resonance frequency, the acoustical output power has a maximum. The impedance of the speaker will also have a maximum. In the case of a moving coil loudspeaker, this impedance maximum arises from the movement of the voice coil (which is part of the speaker cone) in the magnetic field. A counter electromagnetic potential is generated, which opposes the applied signal voltage, thus producing a maximum potential drop across the speaker. The impedance is easy to measure using the electric circuit shown in Fig. 7. The potential drop across the speaker, V_L, is given by

$$V_L = V \frac{R_L}{(R_L + R)} , \qquad (3.1)$$

(a) CONE SHOWING FOUR RADIAL NODES

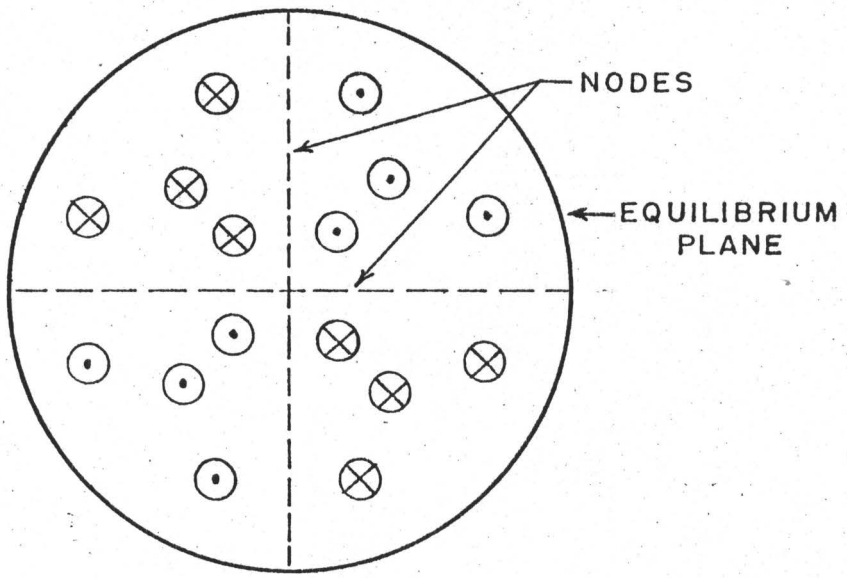

(b) CONE SHOWING TWO CIRCULAR NODES

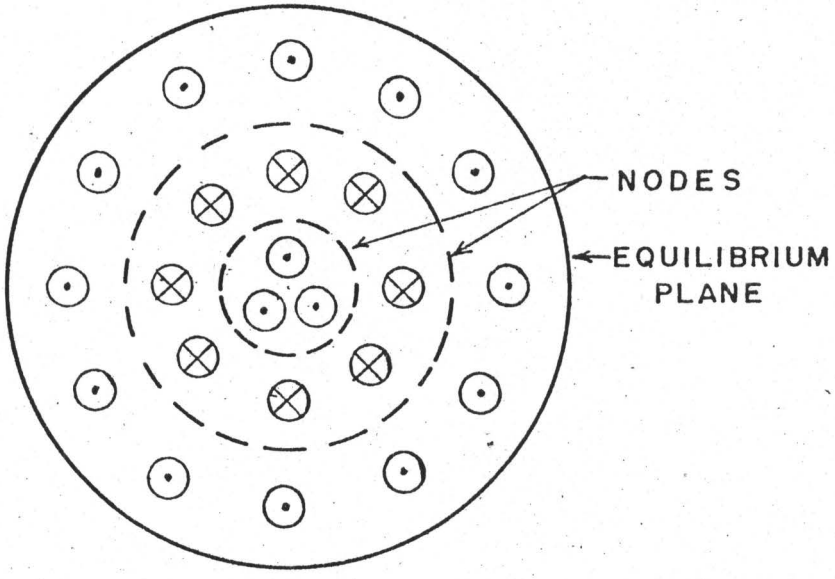

⊙ = DISPLACEMENT OUT OF EQUILIBRIUM PLANE

⊗ = DISPLACEMENT INTO EQUILIBRIUM PLANE

Fig. 6: The instantaneous vibrational displacements for radial and symmetrical, circular mode of a cone

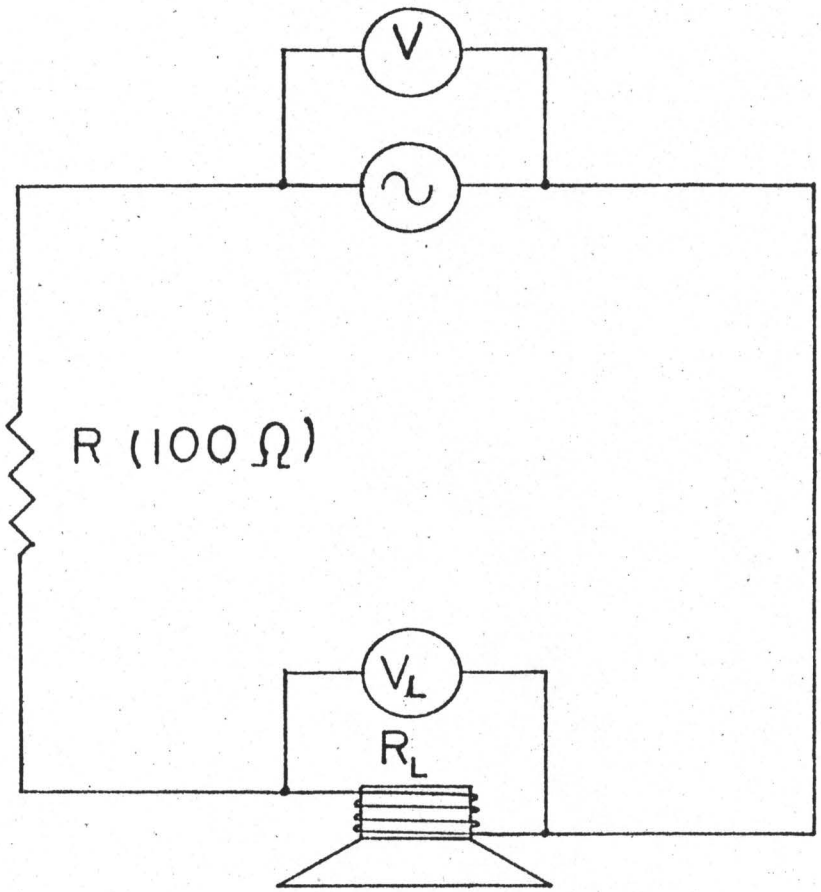

Fig. 7: The electrical circuit for resonance frequency determinations

where R is the resistance of the resistor connected in series with the speaker, R_L is the impedance of the speaker, and V is the signal voltage. By chosing

$$R_L << R, \tag{3.2}$$

Eq. (3.1) can be simplified to give

$$V_L = VR_L R^{-1}. \tag{3.3}$$

Keeping V and R constant, a maximum in the speaker impedance can be measured in terms of a maximum in the potential drop across the speaker. A maximum in the potential drop across the speaker defines a speaker resonance frequency. Application of this method considerably simplified finding the location of the resonance frequencies necessary for the holographic mode structure studies in this report.

CHAPTER 4

MAXIMIZATION OF THE HOLOGRAPHIC, INTERFEROMETRIC PARAMETERS

4.1 Introduction

To obtain a good hologram of a vibrating object, considerable attention has to be given to

(i) the spatial and temporal coherence of the radiation used,

(ii) the environmental and mechanical stability of the holographic system,

(iii) the absolute and relative intensities of the illuminating radiation, and

(iv) the interferometric sensitivity required to measure the vibrational amplitudes.

In this chapter, each topic is considered separately. The resulting parameters used are defined by Fig. 1 and the optimum experimental values for this work are summarized in Table II.

4.2 Temporal and Spatial Coherence Requirements

Whenever a hologram is to be taken we must assure that the reference beam and the object beam in Fig. 1 are both temporally and spatially coherent (see below). If this condition is not fulfilled, then a sharp set of interference fringes will not be formed in the photographic emulsion. Consequently, a holographic picture cannot be

Table II

Experimental Parameters

Parameters	Angle	Distances(cm)
Spatial filter-beam splitter, $\overline{AD}$		51
Beam splitter-object mirror, $\overline{DE}$		86
Beam splitter-reference mirror, $\overline{DF}$		37
Object mirror-object, $\overline{EC}$		30
Object-holographic plate, $\overline{CF}$		23
Reference mirror-holographic plate, $\overline{FB}$		100
Object mirror-object-holographic plate, (EOB)	47°	
Object-holographic plate-reference mirror, (OBF)	27°	
Beam-splitter-object mirror-object, (DEO)	24°	

He-Ne laser: "Spectra Physics", Model 124A, 19 mW uniphase at 6328 Å

Spatial filter: focal length 9 mm, 10 μm diameter pinhole

High density anti-vibration cast-iron table: 96" x 36" x 6"

reconstructed.

Complete temporal coherence or monochromaticity is only possible for radiation with zero spectral linewidth. A source with a finite spectral width will not have a fixed phase relationship at all points in space for all frequencies, which is a necessary requirement for coherence. It can be shown that good temporal coherence exists for distances less than

$$L = \frac{C}{2\Delta f_D} , \tag{4.1}$$

where L is the coherence length, C is the speed of light, and Δf_D is the linewidth of the source. For the He-Ne laser, L is approximately 11 cm.[17] The difference in path length between the reference beam and the object beam was therefore kep below 5 cm as can be seen from Table II.

The radiation is spatially coherent if it can be focussed to a "point". This condition is satisfied by any of the transverse operating modes of the laser. Due to its uniform characteristics the TEM_{oo} mode is preferred. This can be achieved by carefully adjusting the characteristics of the laser. A spatial filter, which consists of two lenses, together with a pinhole at their common focus, ensures a relatively uniform beam intensity. The pinhole minimizes stray light, diffraction patterns produced by impurities of the optical components, and internal reflections preceding the spatial filter. The spatial filter also functions as a beam expander, to produce a beam with a reasonable diameter for object illuminations.

4.3 Environmental and Mechanical Stability Requirements of the Holographic Systems

In order to produce a good hologram, the optical path lengths of object and reference beams should not change during exposure by more than a fraction of the wavelength of the radiation source. Mechanical vibrations of the components and air disturbances (which can be of thermal or barometric origin) have to be kept to a minimum. A loudspeaker cone not only vibrates but also produces acoustical disturbances in the air. Consequently, considerable care has to be excercised to obtain a reasonably stable system.

To achieve mechanical stability, a heavy cast-iron optical table is used which is supported by six airplane inner tubes. This forms an effective antivibration table, which eliminates possible building and optical equipment vibrations. All elements of the holographic system are securely fastened to the optical bench by magnetic mounts or by bolts. Operating the speaker at high frequencies also assists in achieving the necessary mechanical stability.

To reduce external air disturbances, the system was partly enclosed in an environmental control box employed previously by Jonkheere.[18] The optical path was kept to a minimum and the optical paths under direct acoustical influence were reduced to the lowest possible value. The distances between the speaker and the object mirror and the distance between the speaker and the photographic plate could only be reduced to about 23 cm, the value in Table II. A further reduction of these distances produced holograms of very low quality since the sound waves were strong enough to disturb the mechanical

stability of the object mirror and the photographic plate. Before a holographic exposure is made the system is allowed a three minute rest period in order to eliminate any external table vibrations and air disturbances.

4.4 Absolute and Relative Intensities of the Illuminating Beams

The best reference beam to object beam intensity ratio is about 8:1,[17] and was used in this work. The number of optical elements in the system were minimized to obtain the maximum absolute intensity. This measure increased the quality of the hologram in two ways.

(i) it provided minimum exposure times, and

(ii) the quality of the beams was not degraded by unnecessary components.

Best results were obtained with Agfa-Gevaert-Holotest IOE75, 4" x 5" photographic plates. The optimum exposure time was about four seconds. Reasonable results were obtained using Kodak Holographic Plates, Type 120-02. In this case, optimum exposure times were typically around fifty seconds. All plates were developed for six minutes in Kodak Developer D-19 at a temperature of 20°C, and fixed for six minutes in Kodak Fixer.

4.5 Interferometric Sensitivity Requirements

It was found in Chapter 2 that the vibrational amplitude for the n^{th} destructive interference fringe was given by

$$m_{rHe} = X_{nHe} k(\cos\alpha)^{-1}. \qquad (2.32)$$

It is therefore clear, that in order to measure small vibrational amplitudes, k should be minimized. That is, for a small value of k, a correspondingly small amplitude is measurable. Using

$$k = (\cos\theta)^{-1}, \tag{2.24}$$

and $\theta = 23.5°$ from Table II results in $k = 1.09$. k is therefore a sensitivity determining factor of the holographic system. Another sensitivity determining factor in Eq. (2.32) is α.

The angle α, like k, is independent of the fringe order number n, and should ideally be brought to zero. However, this condition can only be satisfied with a flat vibrating object. For a vibrating cone, angle α would in general assume a different value at different locations on the cone surface. This would mean that, for example, the destructive fringe order number $n = 1$ at different cone surface locations, would correspond to different vibrational amplitudes. This is very undesirable for fast vibrational amplitude calculations. The angle α is, however, approximately constant if we let the axis of symmetry of the speaker cone coincide with line defined by $\alpha = 0°$. Thus antisymmetric interference mode patterns are eliminated or each interference fringe represents the location of constant vibrational amplitudes for the whole cone surface. Interpretation of the interference hologram is therefore very easy. An additional advantage of this arrangement is that the plane defined by the outer rim of the speaker at C (Fig. 3) is parallel to the ellipse at C. Since the ellipse is a set of points of constant object-beam lengths, the temporal coherence is assured for the whole cone surface. It might be noted here

that the interference fringes were located very close to the cone's surface and no focussing problems were experienced for reproduction and measurement purposes.

CHAPTER 5

HOLOGRAPHIC INTERFEROMETRIC RESULTS AND INTERPRETATION

5.1 Introduction

In this study, the vibrational mode structures of an electromagnetic and a piezoelectric high frequency loud speaker cone were investigated. Results are shown in Fig. 8 to Fig. 14 and Fig. 15 to Fig. 23, respectively. The electromagnetic speaker cone had an outer diameter of 8.0 cm and a cone angle of 134°. The piezoelectric speaker cone had an outer diameter of 7.7 cm and a cone angle of 138°. The piezoelectric speaker proved more valuable in the study because it had a very small cone bottom and it had no electrical leads attached to the cone. Clearer mode patterns were therefore produced. Low frequency holographic recordings could not be obtained due to system instabilities. The determination of resonance frequencies as described in Chapter 3 did not produce distinct,well defined resonance peaks and extreme care had to be exercised to obtain approximate resonant frequencies. These are listed in Table III for the piezoelectric speaker. These resonant frequencies proved to be very valuable for obtaining good interferometric holograms. Holograms taken at intermediate frequencies (i.e., between resonances) were of extremely poor quality and showed little evidence of vibrational mode patterns. At frequencies above 10 kHz this effect was less pronounced. The speaker driving frequencies ranged from .1 kHz to 16 kHz. The speakers were operated at normal listening sound levels, except for the

Fig. 8: The vibrational mode pattern of an electromagnetic loud speaker cone driven at a frequency of 0.3 kHz

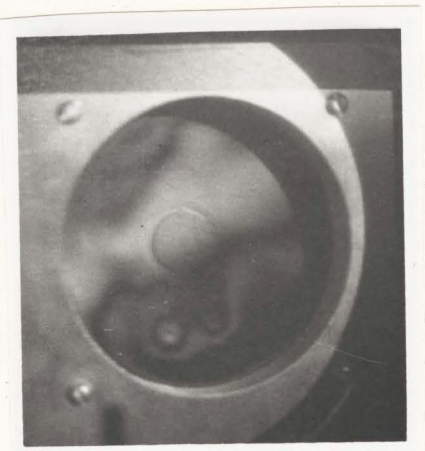

Fig. 9: The vibrational mode pattern of an electromagnetic loud speaker cone driven at a frequency of 0.5 kHz

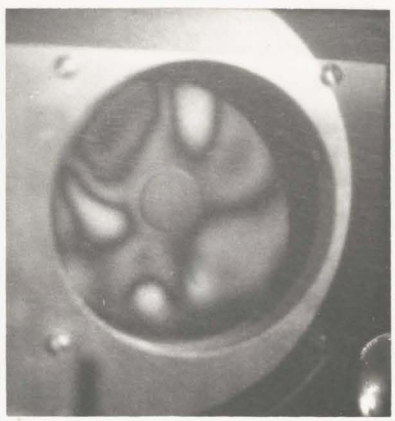

Fig. 10: The vibrational mode pattern of an electromagnetic loud speaker cone driven at a frequency of 1.8 kHz

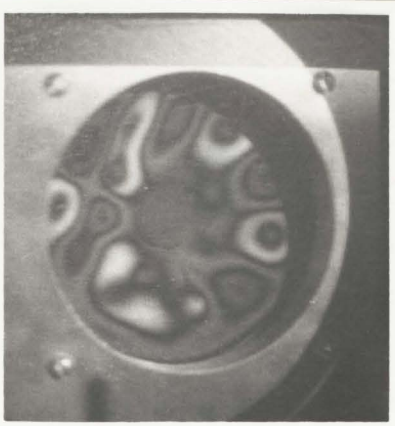

Fig. 11: The vibrational mode pattern of an electromagnetic loud speaker cone driven at a frequency of 2.2 kHz

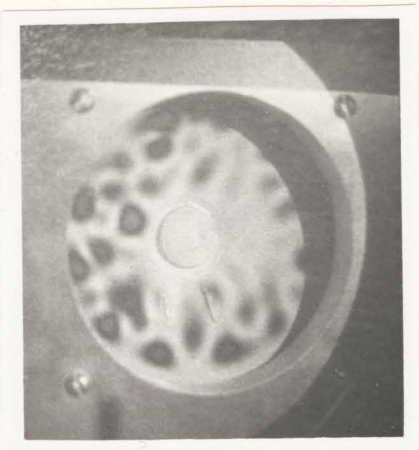

Fig. 12: The vibrational mode pattern of an electromagnetic loud speaker cone driven at a frequency of 4.6 kHz

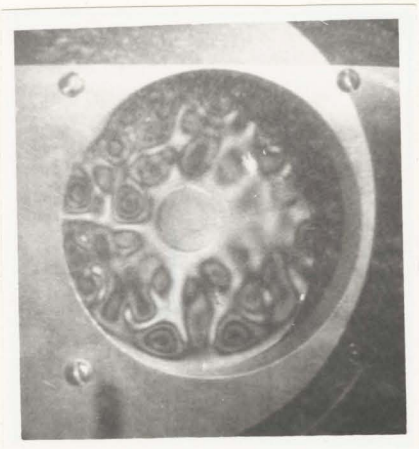

Fig. 13: The vibrational mode pattern of an electromagnetic loud speaker cone driven at a frequency of 4.6 kHz, a high amplitude pattern

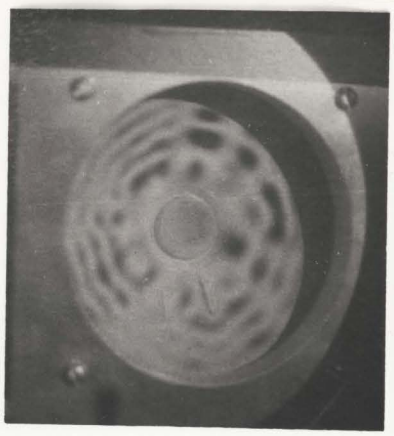

Fig. 14: The vibrational mode pattern of an electromagnetic speaker cone driven at a frequency of 9.6 kHz

Fig. 15: The vibrational mode pattern of a piezoelectric speaker cone driven at a frequency of 3.0 kHz

Fig. 16: The vibrational mode pattern of a piezoelectric speaker cone driven at a frequency of 3.6 kHz

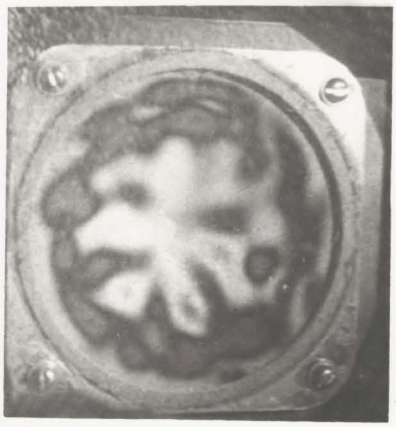

Fig. 17: The vibrational mode pattern of a piezoelectric speaker cone driven at a frequency of 4.3 kHz

Fig. 18: The vibrational mode pattern of a piezoelectric speaker cone driven at a frequency of 5.5 kHz

Fig. 19: The vibrational mode pattern of a piezoelectric speaker cone driven at a frequency of 6.6 kHz

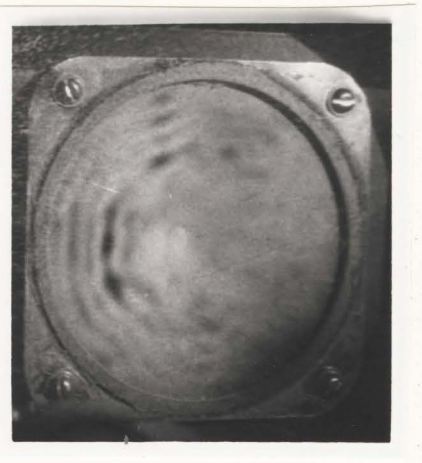

Fig. 20: The vibrational mode pattern of a piezoelectric speaker cone driven at a frequency of 8.2 kHz

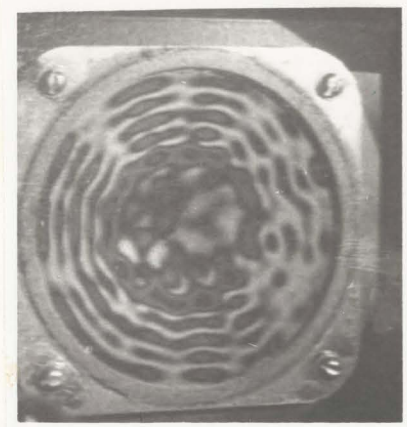

Fig. 21: The vibrational mode pattern of a piezoelectric speaker cone driven at a frequency of 9.6 kHz

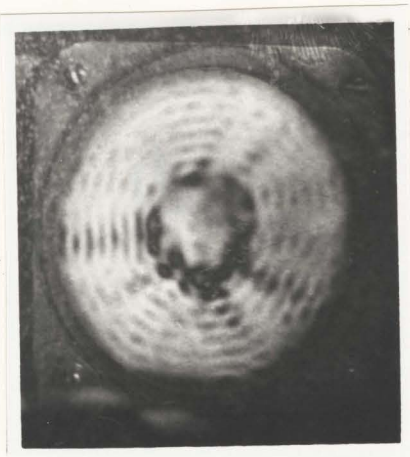

Fig. 22: The vibrational mode pattern of a piezoelectric speaker cone driven at a frequency of 14.0 kHz

Fig. 23: The vibrational mode pattern of a piezoelectric speaker cone driven at a frequency of 15.5 kHz

Table III

Resonance frequencies and modes for a high frequency piezoelectric loudspeaker

Resonance frequency in kHz	Corresponding mode patterns
1.4	4 radial nodes
3.0	7 or 8 radial nodes, 1 circular antinode
3.6	10 radial nodes, 1 circular antinode
4.3	8 radial nodes, 1 or 2 circular antiodes
5.5	12 radial nodes, 3 circular antinodes
6.6	3 circular antinodes
8.2	4 circular antinodes
9.6	5 circular antinodes
14.0	8 circular antinodes
15.5	8 circular antinodes

hologram displayed in Fig. 13. Here the speaker was operated at the maximum possible volume which still produced a clear and undistorted tone.

5.2 Measurement of the Vibrational Cone Amplitudes

In Chapter 2 it was found that the vibrational amplitude was given by

$$m_{rHe} = X_{nHe} k(\cos\alpha)^{-1}, \tag{2.32}$$

where X_{nHe} is given in Table I, $k = 1.09$ and α is approximately 21° and 23° for the piezoelectric and electromagnetic speaker, respectively. With this formula, the calculations of the vibrational amplitudes are very simple. Amplitudes for the first ten interference fringes are summarized in Table IV. The fringe number is counted starting with the fringe closest to a node, which is characterized by its maximum brightness.

The vibrational amplitude at any given location on the cone's surface, at a constant driving frequency increases as the speaker driving potential is increased. A comparison between Fig. 12 and Fig. 13 shows this clearly. At certain surface locations, we can see by counting interference fringes, that by increasing the driving potential, the vibrational amplitude increased from 0.25 μm to 0.70 μm. This increase was approximately proportional to the driving potential. No change of course is observed at nodes. Figure 13 also shows that amplitudes between 0.10 μm and 0.90 μm can easily be measured. At higher amplitudes, distortion sets in. Should it become necessary to measure higher (or lower) vibrational

Table IV

Holographic interferometric measurement parameters

Destructive interference fringe number, n	Cone vibrational amplitude for the electromagnetic speaker, (μm)	Cone vibrational amplitude for the piezoelectric speaker, (μm)
1	.14 (± 2%)	.14 (± 2%)
2	.33	.33
3	.52	.51
4	.70	.69
5	.89	.88
6	1.08	1.06
7	1.27	1.25
8	1.45	1.43
9	1.64	1.62
10	1.83	1.80

amplitudes, then the k-value and possibly the α-value would have to be adjusted accordingly.

5.3 Discussion of the Observed Vibrational Cone Amplitude Patterns of an Electromagnetic Loudspeaker

The electromagnetic speaker is treated first. This speaker did not produce well defined resonance mode patterns due to the relatively large driving element at the centre of the cone and also due to the driving coil connections. These electrical leads are directly attached to the speaker cone and therefore inhibit possible vibrations. Vibrational amplitudes in regions adjacent to the electrical leads were typically below 0.14 μm, compared to amplitudes as high as 0.80 μm at other locations, as shown in Fig. 8 to Fig. 14.

It was found that for driving frequencies below 1 kHz (Fig. 8 and Fig. 9) the speaker cone moves as a whole. At frequencies between 1 kHz and 4 kHz predominantly radial modes were obtained (Fig. 10 and Fig. 11). The number of radial nodes increased with the driving frequency. Frequencies between 4 kHz and 16 kHz produced mainly circular modes (Fig. 12, Fig. 13, and Fig. 14). The number of circular antinodes increased steadily with increasing frequency. At a driving frequency of 9.6 kHz (Fig. 14) four circular antinodes were observed. At 14.5 kHz seven circular antinodes were produced. Vibrational amplitudes above 16 kHz were too small to be recorded with holographic parameters used in this study.

5.4 Discussion of the Observed Mode Patterns of a Piezoelectric Loudspeaker

The piezoelectric loudspeaker showed the best results concerning cone-vibration characteristics because of its highly symmetrical construction. Completely symmetrical interference patterns, however, could not be obtained. It can be seen that the interference pattern showed considerable disturbances in the bottom, right corner of the speaker (Fig. 17 to Fig. 23). A close inspection of the speaker cone revealed that the cone was locally not attached to the annular surround of the speaker. This illustrates that any flaws in the cone structure can easily be detected by time-averaged holographic interferometry.

As in the case of the electromagnetic speaker, the cone moved as a whole for driving frequencies below 1 kHz. For driving frequencies between 1 kHz and 4 kHz, mainly radial mode patterns were produced. For frequencies between 4 kHz and 16 kHz, circular modes became increasingly important (Table III).

The main feature of the cone mode pattern as illustrated in Fig. 17 to Fig. 23, is that they all show a central cone region with only radial modes, surrounded by an area of high vibrational activity, which is called the main circular antinode, which in turn is surrounded by a number of circular antinodes of smaller amplitudes. A typical amplitude of the dominant circular antinode is 0.30 μm compared to an average amplitude of 0.15 μm for the regular circular antinodes. The dominant circular antinode radius decreases steadily as the driving frequency is increased (Table V). The data actually obtained suggests a linear relationship between frequency and antinode radius, to a first

order approximation (Fig. 24).

The average distance between circular antinodes varies only slightly with frequency. At a driving frequency of about 5 kHz, the distance between circular antinodes is found to be 0.45 cm, compared to 0.30 cm for driving frequencies around 15 kHz.

Table V

Dominant circular antinode radii measured

Speaker driving frequency (kHz)	radius of dominant circular antinode (cm)
3.0	2.7 ± .1
4.3	2.5 ± .1
5.5	2.1 ± .1
6.6	2.0 ± .1
8.2	1.9 ± .1
9.6	1.7 ± .1
14.0	1.05 ± .1
15.5	0.90 ± .1

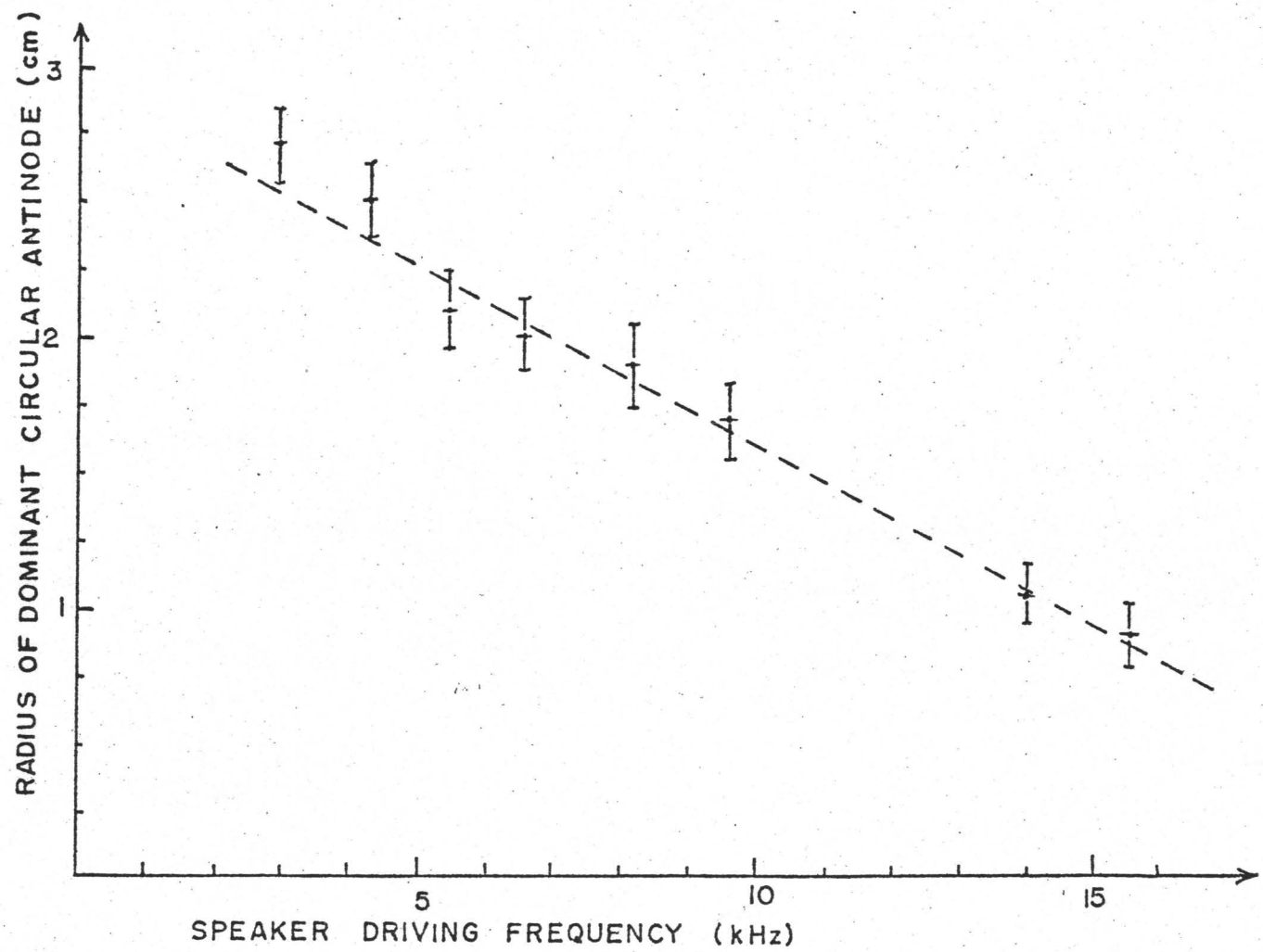

Fig. 24: Speaker driving frequency dependence on the radius of the dominant circular antinode of the piezoelectric speaker

CHAPTER 6

CONCLUSION

Time-averaged holographic interferometry is a very good method for the analysis of high frequency loudspeaker cones. The vibrational amplitudes of the observed speaker cones were as high as 0.8 μm, which was the range for application of holographic interferometry. The usable lower boundary was around 0.1 μm and the upper boundary around 0.9 μm. It was found that the high frequency loudspeakers investigated had an effective frequency range from 0.3 kHz to 16 kHz.

Up to driving frequencies around 1 kHz, the speaker cones moved as a whole. Frequencies between 1 kHz and 4 kHz mainly produced radial modes of increasing number. For frequencies between 4 kHz and 7 kHz, a mixture of radial and circular mode was exhibited, while for frequencies above 7 kHz, circular modes dominated the vibrational amplitude patterns.

Holographic interferometry proved to be a sensitive nondestructive cone quality test, which quite readily showed any flaws in the speaker cone.

Holographic time-averaged interferometry can be an important complementary method used in optimum speaker design such as maximizing speaker efficiency. Holographic interferometry provides the tool for fast and complete vibrational amplitude measurements, necessary for the design of high quality loudspeakers.

REFERENCES

1. B.P. Hildebrand, K.A. Haines, "Multiple-Wavelength and Multiple Source Holography Applied to Contour Generation", J. Opt. Soc. Amer. 57, 155, (1967).
2. K. Snow, R. Vanderwarker, "Application of Holography to Interference Microscopy", Appl. Optics 7, 549, (1968).
3. R.W. Evans, "Assessment of the Strength of Cathode Ray Tubes by Time-Averaged Holographic Interferometry", Optics and Laser Technology 6, 177, (1974).
4. M. Ross, Laser Applications, Academic Press, New York, 1971, p.42.
5. H. Bjelhagen, "Holographic Time-Averaged Vibration Study of a Structure Dynamic Model of an Airplane Fin", Optics and Laser Technology 6, 117, (1974).
6. R.L. Powell, K.A. Stetson, "Interferometric Vibration Analysis by Wavefront Reconstruction", Journal of the Optical Society of America 55, 1593, (1965).
7. E.N. Leith, J. Upatnieks, "Recent Advances in Holography", Progress in Optics 6, 3, (1967).
8. N. Abramson, "The Holo-Diagram: A Practical Device for Making and Evaluating Holograms", Applied Optics 8, 1235, (1969).
9. N. Abramson, "The Holo-Diagram II: A Practical Device for Information Retrieval in Hologram Interferometry", Applied Optics 9, 97, (1970).

10. H. Bjelkhagen, "Simplified Interpretation of Interference Fringes Obtained by Time-Average Holography", Optics and Laser Technology 5, 172, (1973).

11. K.A. Haines and B.P. Hildebrand, "Surface Reformation Measurements Using the Wavefront Reconstruction Technique", Applied Optics 5, 595, (1966).

12. J.E. Sollid, "Holographic Interferometry Applied to Measurements of Small Static Displacements of Diffusely Reflecting Surfaces", Applied Optics 8, 1587 (1969).

13. J.E. Sollid, "Translational Displacements Versus Reformation Displacements in Double Exposure Holographic Interferometry", Optics Communications 2, 282, (1970).

14. D. Bijl and R. Jones, "A New Theory for the Practical Interpretation of Holographic Interference Patterns Resulting from Static Static Surface Displacements", Optica Acta 21, 105, (1974).

15. N.W. McLachlan, LoudSpeakers, Dover Publications, Inc., New York (1960).

16. J. Moir, High Quality Sound Reproduction, Chapman and Hall Ltd., London (1958).

17. J. Kuperman, Holographic Interferometry, M.Eng. Project, Report B, McMaster University (1973) (unpublished).

18. M.T.A. Jonkheere, "Resolution in Holography, M.Eng. Project, Report B, McMaster University (1972) (unpublished).